Biogeochemistry and microbial diversity in the marine cavity beneath the McMurdo Ice Shelf, Antarctica

Trista J. Vick-Majors,[1] Amanda Achberger,[2] Pamela Santibáñez,[1] John E. Dore,[1] Timothy Hodson,[3] Alexander B. Michaud,[1] Brent C. Christner,[2] Jill Mikucki,[4] Mark L. Skidmore,[5] Ross Powell,[3] W. Peyton Adkins,[2] Carlo Barbante,[6] Andrew Mitchell,[7] Reed Scherer,[3] John C. Priscu*[1]

[1]Department of Land Resources and Environmental Sciences, Montana State University, Bozeman, Montana
[2]Department of Biological Sciences, Louisiana State University, Baton Rouge, Louisiana
[3]Department of Geological and Environmental Sciences, Northern Illinois University, DeKalb, Illinois
[4]Department of Biology, Middlebury College, Middlebury, Vermont
[5]Department of Earth Sciences, Montana State University, Bozeman, Montana
[6]Institute for the Dynamics of Environmental Processes – CNR, Department of Environmental Sciences, University of Venice, Venice, Italy
[7]Department of Geography and Earth Sciences, Aberystwyth University, Ceredigion, UK

Abstract

Ice shelves surround ∼ 75% of Antarctica's coastline and are highly sensitive to climate change; several have recently collapsed and others are predicted to in the near future. Marine waters beneath ice shelves harbor active ecosystems, while adjacent seas can be important areas of bottom water formation. Despite their oceanographic significance, logistical constraints have resulted in few opportunities to directly sample sub-ice shelf cavities. Here, we present the first data on microbial diversity and biogeochemistry beneath the McMurdo Ice Shelf (MIS) near Ross Island, Antarctica. Physicochemical profiles obtained via a 56 m deep borehole through the MIS revealed three vertically layered water masses (Antarctic Surface Water [AASW], Ice Shelf Water [ISW], and modified High Salinity Shelf Water [mHSSW]). Metabolically active, moderately diverse (Shannon diversity from 2.06 to 5.74) microbial communities were detected in the AASW and mHSSW. Heterotrophic bacterial production and dissolved organic matter concentrations were higher (12–37% and 24%, respectively) in mHSSW relative to AASW. Chemoautotrophic production was 5.3 nmol C L^{-1} d^{-1} and 6.0 nmol C L^{-1} d^{-1} in the AASW and mHSSW, respectively. Phytoplankton cells were more abundant and larger in the mHSSW sample relative to the AASW, which indicates sinking of phytoplankton produced in surface waters and, together with southerly flowing currents (0.09–0.16 m s^{-1}), horizontal advection of phytoplankton from McMurdo Sound. Advected phytoplankton carbon together with in situ chemoautotrophic production provide important sources of organic matter and other reduced compounds to support ecosystem processes in the dark waters in the ice shelf cavity.

Ice shelves, which form where glaciers leave the land and float on the ocean surface, cover more than 1.5×10^6 km^2 of coastal ocean in Antarctica (Rignot et al. 2013). Yet, only a few studies have directly measured physical or biological processes beneath Antarctic ice shelves, in the sub-ice shelf marine waters (e.g., Azam et al. 1979; Riddle et al. 2007;

Robinson et al. 2010; Carr et al. 2013). The Ross Ice Shelf (RIS) is the most extensive ice shelf on the planet, accounting for about one-third of the surface area of all Antarctic ice shelves (Fox and Cooper 1994; Depoorter et al. 2013). The RIS covers about half of the Ross Sea, an important area of Antarctic Bottom Water formation, which is vital to the global-scale thermohaline circulation (Jacobs et al. 1970; Budillon et al. 2011). The McMurdo Ice Shelf (MIS) comprises the northwestern portion of the RIS, and although they form a unified sub-ice shelf cavity and are often referred to as a single entity, the MIS originates from different source glaciers than the main body of the RIS (Robinson et al. 2010). The RIS front is typically > 300 m thick and presents a significant inflow barrier to the sub-ice cavity, whereas the

*Correspondence: jpriscu@montana.edu

Additional Supporting Information may be found in the online version of this article.

This article was published online 30 November 2015. A footnote stating that the change updated in affiliation 2. This notice is included in the online and print versions to indicate that both have been corrected.

thinner ($\sim$ 20–100 m) MIS front provides an important hydrologic conduit linking the waters of the Ross Sea to the sub-RIS cavity (Robinson et al. 2010). Waters beneath the RIS are also influenced by subglacial water from continental Antarctica, making the sub-ice shelf waters an important intermediate between the open Ross Sea and subglacial outflow from the Antarctic continent (Horgan et al. 2013).

The Ross Sea is one of the most biologically productive and best-studied marine regions in Antarctica (Smith et al. 2012). Multiple studies have documented the onset of rapid phytoplankton growth during spring concurrent with the loss of winter sea-ice cover (Arrigo and McClain 1994; Smith and Gordon 1997; Arrigo and van Dijken 2004). The annual phytoplankton bloom peaks in surface waters between mid-December and early-January, with chlorophyll *a* (Chl *a*) concentrations in excess of 10 μg L^{-1} (Smith and Gordon 1997). The bloom is dominated initially by *Phaeocystis antarctica* (Smith and Gordon 1997) followed by a mixed diatom assemblage (Arrigo 1999). The summer phytoplankton blooms are sustained by high nutrient levels and shallow mixed layers initiated by melting sea-ice (Smith and Comiso 2008). Decomposition of phytoplankton biomass in this region is associated with one of the largest blooms of bacterioplankton recorded, reaching biomass levels of > 10 mmol C m^{-2} (Ducklow et al. 2001). This productive sea comprises the source of the sub-MIS waters, via McMurdo Sound (Robinson et al. 2010).

In contrast to the relatively well-studied Ross Sea, sub ice-shelf cavities (marine waters beneath ice-shelves) have received far less attention, largely due to logistical constraints associated with accessing the ocean beneath thick, floating ice. The first oceanographic data from beneath the MIS was collected in 2003 and revealed net transport from McMurdo Sound to the MIS cavity, a diurnal tidal cycle, and evidence for tidally driven melting near the ice shelf front (Robinson et al. 2010). The Ross Ice Shelf Project (in 1977; Clough and Hansen 1979) was the first to make oceanographic measurements (Gilmour 1979; Jacobs et al. 1979; Williams and Robinson 1979) and detect sub-ice shelf biological communities (Azam et al. 1979; Lipps et al. 1979) beneath the RIS (420 m ice thickness) at Station J9, 450 km from the edge of the RIS. Microorganisms in the water column and seafloor sediments at Station J9 metabolized added organic substrates (Azam et al. 1979) and dark carbon dioxide (CO_2) fixation (1.5 g C m^{-2} yr^{-1}) was attributed to the activity of nitrifying microorganisms (Horrigan 1981). Underwater camera observations and traps yielded fish and crustaceans (Lipps et al. 1979), suggesting the existence of an active food web under the ice shelf, although the benthic community consisted mainly of scavengers. More recently, samples from beneath the RIS and MIS near Ross Island led to the discovery of a new species of sea anemone that embeds in and inhabits the base of the ice shelf (Daly et al. 2013), and provided information on the microbial commu-

nity composition of marine sediments below this region of the ice shelf (Carr et al. 2013). Underwater camera observations showed that a diverse benthic community, unlike that detected at Station J9 beneath the RIS, exists beneath the Amery Ice Shelf (Post et al. 2014). These studies suggest that sub-ice shelf biota are involved in Southern Ocean biogeochemical processes, but that we have a poor understanding of both the diversity of life and habitats beneath ice shelves.

As Antarctic ice shelves are increasingly threatened with collapse induced by changing climate (Joughin et al. 2014; Wouters et al. 2015), the need to develop an understanding of sub-ice shelf biogeochemical processes becomes progressively more important. Studies following the breakup of the Larsen A and B Ice Shelves documented changes in biological CO_2 pumping mediated by water column primary production (Bertolin and Schloss 2009) and disruption and succession of benthic communities beneath the newly open water (Domack et al. 2005; Fillinger et al. 2013). Still, a paucity of baseline data limits the context within which the ramifications of ice shelf collapse for biogeochemical processes in the Southern Ocean can be interpreted. Here, we integrate physical and chemical data with the first microbiological data obtained from the sub-MIS water column. Our results identify biogeochemical linkages between the Ross Sea via McMurdo Sound and the dark sub-ice environment beneath the MIS and RIS.

Methods

Site description

The Ross Ice Shelf stretches $\sim$ 850 km from the Antarctic coast to the open ocean, with water column depths ranging from $\sim$ 50 m to $\sim$ 1000 m (Greischar and Bentley 1980). The MIS comprises the thinnest area of the ice shelf, with ice thicknesses generally < 100 m thick at MIS compared with up to > 800 m thick near the southern extent of the RIS (most of the RIS is $\sim$ 200–250 m thick; Griggs and Bamber 2011). A coastal current flows along the front of the RIS until it reaches Ross Island, where some of the water turns north along the Victoria Land coast, and some flows south, through the eastern part of McMurdo Sound and beneath the MIS (Barry 1988).

Our drill site was located on the MIS (77.8902 S, 167.0083 E; Fig. 1) near Ross Island, approximately 8 km from the edge of the transition from ice shelf to the seasonal and multi-year fast sea-ice of McMurdo Sound and $\sim$ 2 km from the ANDRILL HWD-1 site described by Robinson et al. (2010) and Robinson (2004), which we use for comparison in this article. At the time of sampling, the transition from sea-ice to the open water of McMurdo Sound was approximately 48 km to the north of the sampling site. The 56 m deep borehole ($\sim$ 60 cm diameter) that penetrated into the sub-ice shelf cavity was created with a clean access hot water drill (Blythe et al. 2014; Burnett et al. 2014; Rack et al. 2014)
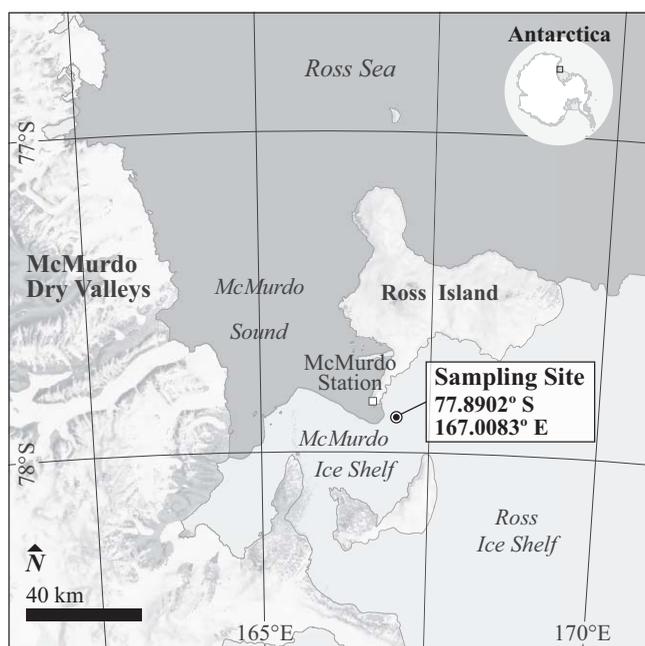
Fig. 1. Sampling site location. Map by Bradley Herried, Polar Geospatial Center.

on 18 December 2012. The sub-ice shelf cavity is defined as the ocean beneath the ice-shelf. The water column depth below the borehole was 872 m from the ice-water interface (928 m from the ice surface) to the seafloor. All depths are reported from the bottom of the ice shelf (i.e., the ice-water interface). MODIS satellite imagery from around the time of sampling (not shown; data available from the U.S. Geological Survey EarthExplorer) indicated that we did not collect samples during the Ross Sea phytoplankton bloom.

Physical and chemical parameters

Depth profiles of temperature and conductivity were measured with a SBE 19plusV2 SeaCAT Profiler CTD (Seabird Electronics) sonde. Potential temperature relative to the surface was derived according to UNESCO equations (IOC, SCOR and IAPSO 2010). Water masses observed in the study area were characterized according to Stover (2006) and Jacobs and Fairbanks (1985) (see also Celussi et al. 2010) as: (1) Antarctic Surface Water (AASW) having potential temperature above the freezing point with relatively low salinity (34.2 and 34.4); (2) Ice Shelf Water (ISW) with potential temperature below the surface freezing point and salinities between 34.5 and 34.7, and (3) modified High Salinity Shelf Water (mHSSW) possessing potential temperature near the surface freezing point with salinities between 34.6 and 34.8. These water masses were graphically identified using Ocean Data View 4.5.6 (Schlitzer 2013), as shown in Supporting Information Fig. S1. Current velocity and direction were obtained with a Contros Oceanline HS-2X series electromag-

netic current meter and the appearance of the surface sediments was documented with an attached camera.

Discrete water samples were collected through the borehole with a 10 L General Oceanics Niskin bottle (AASW [30 m] sample) and a 5 L Go-Flo bottle (mHSSW [850 m] sample). Both sampling bottles were disinfected with 3% hydrogen peroxide before deployment. The water was decanted immediately through acid leached silicone tubing into appropriate vessels. Samples for dissolved oxygen and dissolved inorganic carbon (DIC) were stabilized on site with a final concentration of sodium azide (0.05% w/v), potassium iodide (0.5% w/v), sodium hydroxide (1.5% w/v) (dissolved oxygen) or chloroform (DIC). All water samples were stored at $\sim 4°C$ in the dark until return to McMurdo Station (MCM) for processing (~ 4 h).

Shallow sediment samples were collected from the top surface of a geothermal probe that penetrated the surface sediments in an operational test, and the resulting data are reported qualitatively. Diatom frustules in fine-grained sediments were processed using standard micropaleontological techniques (e.g., Scherer 1991), using 15% H_2O_2 and mounted as strewn slides in Norland optical adhesive for light microscopy.

Samples for DOC and three dimensional spectrofluorometric characterization of organic matter (excitation-emission matrix spectroscopy; EEMS) were decanted into 1% hydrochloric acid and deionized water rinsed fluorinated high density polyethylene (HDPE) carboys (Thermo Scientific, Nalgene, Waltham, Massachusetts) and filtered through acid-leached and combusted (> 4 h at 450°C) 25 mm glass fiber filters (GF/F, effective retention size 0.7 μm). The filtrate was collected in acid washed and combusted (> 4 h at 450°C) 125 mL amber borosilicate glass bottles fitted with polytetrafluoroethylene (PTFE) lined caps and stored at 4°C until analysis. DOC concentrations were determined using a Shimadzu TOC-V Series TOC analyzer following acidification with hydrochloric acid to pH ≤ 2 to remove inorganic carbon as CO_2.

EEMS were determined with a Horiba Jobin Yvon Fluoromax-4 Spectrophotometer (Horiba, Ltd., Japan) equipped with a Xe light source using a 1 cm path length quartz cuvette. Excitation data were measured every 10 nm from 240 nm to 450 nm, and emission data every 2 nm from 300 nm to 560 nm. Measurements were corrected for background (0.2 μm filtered Milli-Q water) and Raman scattering, and for inner-filter effects using absorbance spectra collected between 190 nm and 1100 nm with a Genesys 10 Series Spectrophotometer (1 cm path length, Thermo Scientific) as described by McKnight et al. (2001). The following indices were derived to reveal the character of the DOC: (1) Fluorescence Index (the ratio of the emission at 470 nm to the emission at 520 nm at an excitation of 370 nm; McKnight et al. 2001; Cory and McKnight 2005), (2) Freshness Index (the emission at 380 nm divided by the maximum emission between 420 nm and 435 nm at an excitation

370 nm; Huguet et al. 2009), and (3) Humification Index (the area of the peak under emission 435–480 nm divided by the peak area under emission 330–345 nm; Zsolnay et al. 1999). To compare fluorescence intensities in the two samples, standardized maximum fluorescence was calculated as follows: (value-min)/(max-min), where "value" is the maximum fluorescence in the sample, and "max" and "min" are the maximum and minimum fluorescence for the two samples combined.

Suspended matter collected on the filters from DOC and EEMS filtration was stored frozen ($-20°C$) in the dark until acid-fuming (to remove inorganic C) and analysis of particulate organic C (PC) and nitrogen (PN) on a CE Instruments Flash EA 112 (ThermoQuest, San Jose, California). Dissolved oxygen and DIC were measured in MCM using the azide modification of the mini-Winkler titration and infrared gas analysis of acid sparged samples, respectively, according to the limnological methods used by the McMurdo LTER (http://www.mcmlter.org/data_methods2.htm).

Samples for dissolved inorganic nutrients (soluble reactive phosphorus [SRP], nitrate + nitrite [N+N], and ammonium [NH_4^+] were filtered through combusted GF/F filters into 1% hydrochloric acid leached and deionized water rinsed HDPE bottles and frozen at $-20°C$ until analysis. The concentrations of these compounds were determined colorimetrically according to Strickland and Parsons (1968) and Solórzano (1969).

Biological parameters

Chl *a* concentrations were determined on 200 mL samples filtered onto 25 mm diameter GF/F filters; the filters were stored at $-20°C$ in the dark immediately on return to MCM. The samples were extracted in 90% acetone (v:v; acetone:water) for $\sim$ 24 h in the dark at 4°C and analyzed with a calibrated fluorometer (Turner 10-AU-10) as described by Welschmeyer (1994).

Dark carbon fixation (chemoautotrophy) was determined on quadruplicate live and trichloroacetic acid [TCA; $\sim$ 5% final concentration] killed 40 mL samples (Christner et al. 2014). The samples were incubated in the dark in glass bottles filled to the top (no head-space) and capped with PTFE lined caps. Each sample was amended with ^{14}C-bicarbonate (stock solution = 114.41 μCi mL^{-1}) to a final radioactive concentration of 10 μCi mL^{-1} and incubated in the dark at 4°C for 94 h. Long incubation times and high specific activity substrates were used in anticipation of low rates of biological activity in the sub-ice shelf cavity, and were similar to those used in other studies aimed at detecting chemoautotrophic carbon fixation (48 h, Horrigan 1981; 168 h, Yakimov et al. 2011). Incubations were terminated by the addition of ice-cold 100% TCA (2.5% final concentration) and size fractionated onto GF/F filters (to capture larger, aggregated and filamentous cells) and 0.2 μm polycarbonate filters (to capture smaller or non-aggregated cells). Filters were placed in 20 mL scintillation vials, acidified with 1.5 mL of 3N HCl and dried

at 60°C. Radioactivity incorporated into cellular carbon retained on the filters was counted on a calibrated scintillation counter after addition of 10 mL Cytoscint ES scintillation cocktail (MP Biomedicals).

Heterotrophic bacterial (where "bacterial" can include bacteria and archaea throughout the text) production was determined using [^{3}H]methyl-thymidine incorporation into DNA (Fuhrman and Azam 1982) and [^{3}H]L-leucine incorporation into protein (Kirchman et al. 1985). Samples (1.5 mL; five live and five TCA killed) were incubated with 20 nM radio-labeled thymidine (specific activity 20 Ci mmol^{-1}) or leucine (specific activity 84 Ci mmol^{-1}) at 4°C in the dark for $\sim$ 20 h. Incubations were terminated by the addition of 100% cold TCA (5% final). Following centrifugation, a series of extractions with cold ($\sim$ 4°C) 5% TCA and cold ($\sim$ 4°C) 80% ethanol were performed and the residual pellet was dried overnight at room temperature. One milliliter of Cytoscint ES scintillation cocktail was added to each vial and the samples were counted on a calibrated scintillation counter. Resulting thymidine and leucine incorporation rates (nM TdR d^{-1} or nM Leu d^{-1}, respectively) at the incubation temperature (4°C) were converted to rates at in situ temperatures ($-1.7°C$ to $-1.9°C$) using energy of activation of 12,600 kcal mol^{-1} determined from Antarctic lakes (Takacs and Priscu 1998). Temperature corrected rates were converted to heterotrophic bacterial production (BP TdR and BP Leu) using published conversion factors of 2.0×10^{18} cells mol^{-1} thymidine (Bell 1993) and 1.42×10^{17} cells mol^{-1} leucine (Chin-Leo and Kirchman 1988) and a cellular carbon content of 11 fg C cell^{-1} (Kepner et al. 1998). Cell specific activity (mg C cell^{-1} d^{-1}) was determined by dividing heterotrophic bacterial production by bacterioplankton cell abundance (see below) for each sample.

Heterotrophic bacterial respiration was measured in the 850 m sample by adding 60 mL of sample water to an autoclaved amber HDPE bottle (Nalgene) followed by the addition of uniformly labeled ^{14}C-L-leucine (specific activity > 300 mCi mmol^{-1}; final leucine concentration 60 nM; final activity 0.0180 μCi mL^{-1}) (del Giorgio et al. 2011). Five-milliliter aliquots of the radiolabeled sample were added to autoclaved 25 mL glass side arm flasks (six live and six TCA killed controls; 250 μL of cold 100% TCA). The top of the flask was sealed with a butyl rubber septum holding a small basket containing a folded GF/C filter suspended above the aqueous phase (Christner et al. 2006); the sidearm was sealed with a butyl rubber septum. Following incubation in the dark for 39 h at 2–4°C, the reactions in live incubations were terminated by injecting cold 100% TCA (final concentration 5%) into the sample through the sidearm which lowered the pH to $\leq$2. β-phenylethylamine (100 μL; Sigma, catalog number P2641) was added to the GF/C filter through the septum with a needle and syringe to trap respired CO_2. Killed samples were maintained at 4°C for 5 d with occasional gentle swirling to liberate and trap all respired

CO_2 from the aqueous phase. Cellular ^{14}C incorporation was determined on the liquid fraction following filtration onto 0.2 μm polycarbonate filters. The GF/C and polycarbonate filters were placed in 20 mL scintillation vials followed by the addition of 10 mL of Cytoscint-ES and the ^{14}C activity was determined using a calibrated scintillation counter. Bacterial growth efficiency was calculated using the leucine respiration data (described above) as ((BP Leu)/(BP Leu + Leu respiration)) × 100. Leu: TdR ratios are based on molar incorporation rates.

Samples for phytoplankton (autofluorescent cells) and bacterioplankton (non-autofluorescent bacteria and archaea) enumeration were preserved with sodium borate buffered formalin (5% v/v) and stored at 4°C in the dark. Samples were filtered through 30 μm mesh using a sterile BD Falcon 12 × 75 mm tube with cell strainer cap to eliminate large particles. Cell density was determined with a PhytoCyt flow cytometer (Turner Designs) at a flow rate of 50 μL min^{-1} and core size of 12 μm. Unstained seawater samples were used for the detection of phytoplankton. Bacterioplankton were enumerated using seawater samples stained with SYBR® Green I (SGI; Molecular Probes; supplied at 10,000X) at a final concentration of 1X original (Marie et al. 2001).

Bacterioplankton cells were identified as a distinct population on a density plot of SGI emission-height (excitation 488 nm, emission 515–545 nm) vs. forward light scatter-area (FSC-A: 0° ± 15°). High nucleic acid (HNA) and low nucleic acid (LNA) bacterioplankton were identified according to the intensity of their SGI emission (Gasol and del Giorgio 2000; Lebaron et al. 2001; Bouvier et al. 2007). Because FSC-A and SGI emission from small phytoplankton cells may overlap with those of stained bacterioplankton, we also examined small phytoplankton (< 2 μm Chl *a* autofluorescing cells) in stained samples by plotting FSC-A vs. orange fluorescence (excitation 488 nm, emission 565–605 nm), blue laser-dependent red fluorescence (excitation 488 nm, emission > 670 nm; Chl *a*) and red fluorescence (excitation 640 nm; emission 650–700). Small phytoplankton cells determined using these criteria were subtracted from the total counts in this region to obtain bacterioplankton cell counts. Bacterioplankton cell counts were verified on selected samples by epifluorescence microscopy of SYBR® Gold-stained cells using the protocol of Lisle and Priscu (2004).

Larger phytoplankton cells (> 2 μm) were enumerated on a density plot of FSC-A vs. Chl *a* using 2 mL of unstained sample. The larger phytoplankton population was divided into subpopulations (*a*, *b*, and *c*) based on density plots of FSC vs. Chl *a*. The presence of each distinct population was verified by measuring the mean emission ratios of red fluorescence/Chl *a* and orange fluorescence/red fluorescence. To determine cell sizes, the larger phytoplankton were also examined with an epifluorescence microscope (Nikon Eclipse 80i) equipped with a Retiga-2000R Fast 1394 camera under blue excitation cube filter (excitation 450–490 nm; emission > 515 nm) following the method of Hillebrand et al. (1999).

Samples were prepared for microscopy by filtering 1.6 mL (30 m sample) and 2.2 mL (850 m sample) through 0.2 μm 13 mm hydrophilic PTFE membrane filters (Millipore, catalog number JHWP013000) and mounting the filters on glass slides with 1:1 (v:v) glycerol/water. Sixty photographs were taken of random fields at 1000X magnification and the diameter of ∼ 200 cells were measured in each sample (standard error < 2% of the mean) using ImageJ software (Schneider et al. 2012).

Gating strategies for the different classes of planktonic cells are available in the MIFlowCyt-Compliant Items (Lee et al. 2008; Supporting Information) and archived with the data at http://www.flowrepository.org under the ID number FR-FCM-ZZK3.

A discrete water sample for nucleic acid extraction was collected in situ at 850 m with a Large Volume Water Transfer System (WTS-LV; McLane Research Laboratories, East Falmouth, Massachusetts). This system was fitted with a stacked 143 mm diameter filter housing that allowed the sample to be size fractionated into 10 μm, 3 μm, and 0.2 μm classes (Supor Membrane filters were used; Pall). This system allowed us to concentrate 295 L of seawater on 142 mm filters during a 4 h in situ deployment. An additional discrete water sample (300 mL) from 30 m was obtained for nucleic acid extraction from a 10 L Niskin bottle sample that was filtered through a 47 mm 0.2 μm Supor membrane filter (Pall). Filters from the WTS-LV were preserved as described previously (Christner et al. 2014) while the entire 47 mm filter from the 30 m sample was placed in a 7 mL cryovial and preserved with 7 mL of a solution of 40 mM EDTA pH 8.0, 50 mM Tris pH 8.3, and 0.73 M Sucrose to prevent cell lysis during storage.

Nucleic acids were extracted from the 10 μm, 3 μm, and 0.2 μm filters from 850 m and the 0.2 μm filter from 30 m using a MO BIO PowerWater DNA Isolation Kit according to the manufactures instructions. The V4 hypervariable region of the small subunit (SSU) rRNA gene was amplified using the primers 515F and 806R (Caporaso et al. 2012) and sequenced on an Illumina MiSeq as described by Christner et al. (2014). Sequence reads were assembled and quality filtered using the Mothur (v1.33.2; Schloss et al. 2009) phylogenetic pipeline following the recommended MiSeq standard operating procedure. Sequences were clustered into operational taxonomic units (OTUs; cluster.split command) based on a pairwise distance matrix (dist,seq) calculated using default settings. OTUs were defined based on 97% sequence similarity cutoff. Preliminary classification of resulting SSU rRNA gene sequences was accomplished using the SILVA database as implemented within the SILVA Incremental Aligner (SINA). Poorly classified sequences were further examined using NCBI Blastn. Statistics were calculated using Mothur (v1.33.2; Schloss et al. 2009) according to Chao (1984), Good (1953), and Magurran (1988). Estimates of diversity and richness include singletons; singletons were
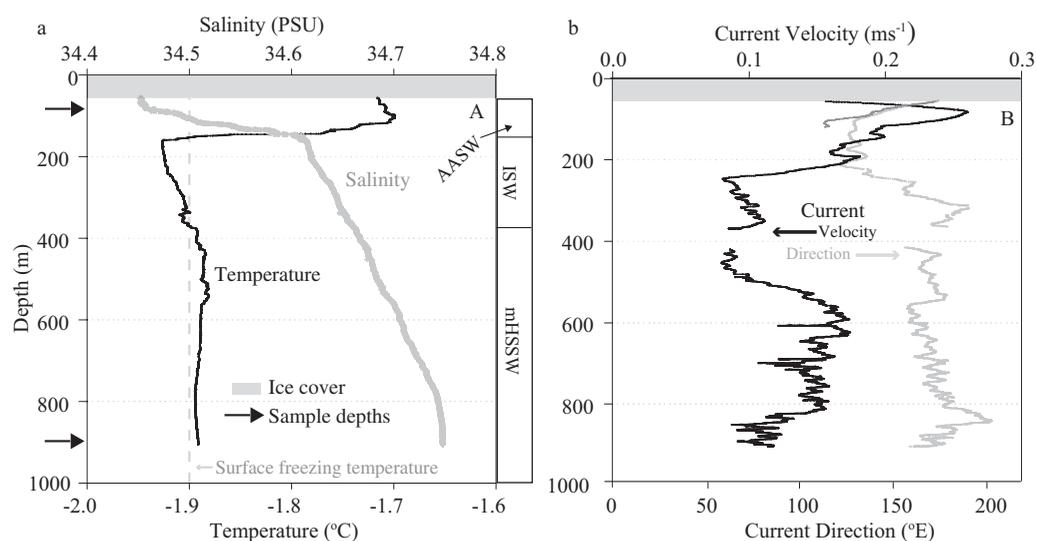
Fig. 2. Profiles of salinity (practical salinity units; PSU) and temperature (**a**), current velocity and direction relative to true north (**b**). Sidebar in panel (**a**) designates three water layers: Antarctic Surface Water (AASW), Ice Shelf Water (ISW), and modified High Salinity Shelf Water (mHSSW).

Table 1. Water column inorganic chemistry from the AASW (30 m) and mHSSW (850 m) water masses sampled.

Sample	DIC mmol L^{-1}	NH$_4^+$ μmol L^{-1}	N+N μmol L^{-1}	SRP μmol L^{-1}	DO μmol L^{-1}
AASW	2.2	0.7	25.1	1.6	333
mHSSW	2.2	0.5	23.0	1.5	367

DIC, dissolved inorganic carbon; N+N, nitrate + nitrite; SRP, soluble reactive phosphorus; DO, dissolved oxygen.

removed from other analyses. SSU sequences obtained from chloroplasts were removed from the analyses. Sequences were uploaded to SRA under accession number PRJNA278982. We note that recent efforts have shown that the primers used in our study underestimate the abundance and diversity of the ubiquitous SAR11 clade of bacteria. A comprehensive discussion of the primers can be found in Appril et al. (2015).

Results

Water column structure

The upper $\sim$ 95 m of the water column (relative to the bottom of the ice shelf) was characterized by relatively warm, less saline water (-1.70°C to -1.89°C, Salinity 34.45–34.61) (Fig. 2a). A colder layer (-1.90°C to -1.93°C) of intermediate salinity (34.60–34.70) was present from $\sim$ 95 m to 315 m. Water below $\sim$ 315 m had temperatures ranging from -1.88°C to -1.90°C and was relatively higher in salinity (34.66–34.75). These water masses were similar to those described previously in this area (Jacobs and Fairbanks 1985; Stover 2006; Celussi et al. 2010): AASW, ISW and mHSSW (Supporting Information Fig. S1). Current flow was generally to the south-southeast with true headings (declination corrected) of 140°, 161° and 162° for the AASW, ISW and

mHSSW layers, respectively (Fig. 2b). Current velocities for these respective layers averaged 0.21 m s^{-1}, 0.11 m s^{-1}, and 0.14 m s^{-1}. Current velocity in the mHSSW layer showed a clear demarcation at 500 m with average velocity in the upper part of this water layer averaging 0.09 m s^{-1} while that below 500 m averaged 0.14 m s^{-1}.

Inorganic chemistry

Concentrations of NH$_4^+$, N+N, and SRP were 40%, 9%, and 7%, respectively, higher in the AASW (30 m sample) relative to the mHSSW (850 m sample). Dissolved oxygen concentrations were 330 μmol L^{-1} and 370 μmol L^{-1}, representing 92% and 97% of air saturation, respectively (Table 1). The concentration of DIC was 2.2 mmol L^{-1} in both samples. The molar ratio of dissolved inorganic N (N+N + NH$_4^+$) to SRP was 16.1 in the AASW and 15.7 mHSSW water layers.

Microbiological characteristics

Bacterioplankton cell densities were 1.2×10^8 cells L^{-1} in the AASW and 1.1×10^8 cells L^{-1} in the mHSSW water layers (Table 2), and similar counts were determined via epifluorescent microscope (data not shown). High-nucleic acid and low-nucleic acid (HNA and LNA) bacterioplankton cells

Table 2. Bacterioplankton and phytoplankton cell counts (cells L^{-1}) determined by flow cytometry for samples collected in the AASW (30 m sample) and mHSSW (850 m sample). Bacterioplankton cell counts are the sum of low nucleic acid (LNA) and high nucleic acid (HNA) cells. Phytoplankton include autofluorescent cells of < 2 μm and > 2 μm diameter. Mean intensity is fluorescence intensity (relative units) per cell excited with the blue laser and read at emission of > 670 nm (Chl a). Phytoplankton > 2 um were divided into three populations: Phyto a, Phyto b, and Phyto c based on size (FSC-A). Total phytoplankton are the sum of all auto-fluorescing organisms.

Sample	Bacterio-plankton ($\times 10^8$)	LNA ($\times 10^7$)	HNA ($\times 10^7$)	Phyto-plankton < 2 μm ($\times 10^6$)	Phytoplankton > 2 μm $\times 10^6$	Mean intensity	Phyto a ($\times 10^6$)	Phyto b ($\times 10^6$)	Phyto c ($\times 10^6$)	Total Phytoplankton ($\times 10^6$)
AASW	1.2	7.5	4.1	1.5	4.5	41836	0.92	2.5	0.59	6.0
mHSSW	1.1	7.2	3.9	0.0010	6.7	54147	0.41	2.9	2.7	6.7

comprised $\sim 35\%$ and $\sim 64\%$ of total bacterioplankton cells in both the AASW and mHSSW, respectively.

Small (< 2 μm) phytoplankton were more abundant in the surface water layer than the deep layer (1.5×10^6 cells L^{-1} in AASW, 1.0×10^4 cells L^{-1} in mHSSW), while the densities of larger (> 2 μm) phytoplankton were 33% higher at depth (Table 2). Microscopic enumeration showed that 83–85% of phytoplankton cells in both samples were *Phaeocystis antarctica*; the remainder consisted of diatoms. Total phytoplankton (large plus small) were 10% higher in the mHSSW relative to densities in the AASW.

Large phytoplankton populations *a, b,* and *c* had distinctly different FSC-A intensities, where greater intensity is related to greater cell size. The mean FSC-A per cell in population *b* was approximately twice that of population *a*. The mean FSC-A per cell for population *c* was approximately twice that of *b* (Fig. 3). The AASW water sample was dominated by population *b* (56% of total phytoplankton), while the mHSSW was dominated by populations *b* and *c* (43% and 40%, respectively; Table 2; Fig. 3). The increase in population *c* relative abundance indicates an increase in cell size (FSC-A) at depth. Microscopic examination of the AASW and mHSSW > 2 μm phytoplankton showed that the between water mass size difference was small (mean $= 3.27$ and 3.44 μm for AASW and mHSSW, respectively) but significant ($t = -4.06$, $n = 410$, $p < 0.001$), supporting the increase in size indicated by the shift toward population *c* dominated phytoplankton at depth. The mean emission ratios of red fluorescence/Chl a fluorescence and orange fluorescence/Chl a fluorescence remained constant within populations indicating that a similar phytopigment composition was present at each depth and only the phytoplankton abundances and sizes changed.

Rates of both Leu and TdR incorporation were higher in the deep mHSSW waters but the difference was proportionally greater for TdR, leading to a lower Leu:TdR molar ratio in the deep waters (14 in the AASW, 9 in the mHSSW; Table 3). In terms of bacterial carbon production, BP-TdR and BP-
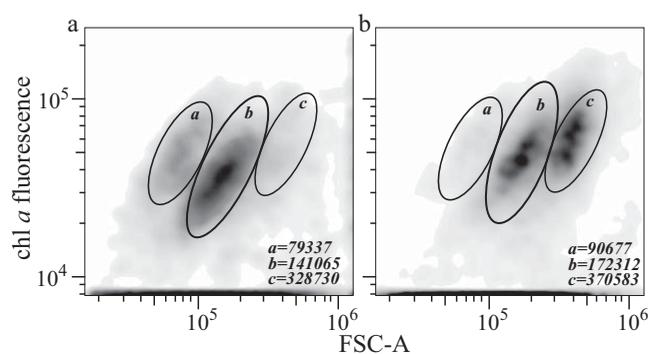

Fig. 3. Density plots of Chl a fluorescence (relative intensity units) vs. forward scatter-area (FSC-A; relative intensity units) in the AASW water (30 m) (**a**) and mHSSW water (850 m) (**b**). Both samples show three distinct populations (a, b, and c) based on differences in FSC-A mean emission intensity for each population. Mean emission intensity for each group is given in the lower right corner of each plot.

Leu ranged from 34.5 nmol C L^{-1} d^{-1} (AASW Leu) to 63.6 nmol C L^{-1} d^{-1} (mHSSW TdR). Cell specific activity was also higher at depth (3.5×10^{-12} mg C $cell^{-1}$ d^{-1} (Leu) and 4.0×10^{-12} mg C $cell^{-1}$ d^{-1} (TdR) in the AASW vs. 4.8×10^{-12} mg C $cell^{-1}$ d^{-1} (Leu) and 6.9×10^{-12} mg C $cell^{-1}$ d^{-1} (TdR) in the mHSSW). Increased activity at depth was also associated with relatively high bacterial growth efficiency (70%). Dark ^{14}C-bicarbonate incorporation ranged from 1.6 nmol C L^{-1} d^{-1} (AASW > 3 μm size fraction) to 3.1 nmol C L^{-1} d^{-1} (mHSSW 0.2–3 μm size fraction) and was higher in the 0.2–3 μm than the > 3 μm size fraction (12% greater in AASW and 6% greater in mHSSW). The summed size fractionated dark ^{14}C-bicarbonate incorporation was greater in the mHSSW (11% difference) and ranged from 9% (mHSSW BP-TdR) to 15% (AASW BP-Leu) of heterotrophic bacterial production.

The molar ratio of particulate organic C:N was slightly higher in the mHSSW (10.5 vs. 10.0), while DOC concentrations were higher in the AASW (42.1 μmol L^{-1}

Table 3. Water column organic chemical composition and microbial activity ($\pm$ propagated standard error) for samples collected in the AASW (30 m) and mHSSW (850 m) water masses. Particulate organic carbon and nitrogen (PC and PN), the molar PC to PN ratio (C:N), dissolved organic carbon (DOC), Chl a, bacterial growth efficiency (BGE) rates of ^{3}H-leucine (Leu) and ^{3}H-thymidine (TdR) incorporation and bacterial production (nmol C L^{-1} d^{-1}) the molar ratio of Leu: TdR (nmol Leu L^{-1} d^{-1}: nmol TdR L^{-1} d^{-1}), rate of ^{14}C-bicarbonate incorporation in the dark (0.2–3 μm and > 3 μm size fractions and the sum of the two size fractions).

| | | | | | | | Leu | | TdR | | | ^{14}C-bicarb nmol C L^{-1} d^{-1} | | |
| | PC | PN | | DOC | Chl a | | nmol | nmol | nmol | nmol | Leu: | 0.2–3 | > 3 | |
Sample	μmol L^{-1}	μmol L^{-1}	C:N	μmol L^{-1}	μg L^{-1}	BGE	L^{-1} d^{-1}	C L^{-1} d^{-1}	L^{-1} d^{-1}	C L^{-1} d^{-1}	TdR	μm	μm	Sum
AASW	28.4	2.2	11.3	42.1	2.4	ND	0.27 (0.02)	35.1 (2.8)	0.022 (0.003)	39.5 (6.0)	12	2.8 (0.2)	2.5 (0.5)	5.3 (0.5)
mHSSW	26.1	1.9	12.0	31.8	2.9	0.7	0.36 (0.08)	47.0 (10.0)	0.035 (0.0003)	63.6 (9.0)	10	3.1 (0.6)	2.9 (1.0)	6.0 (1.0)

ND, not determined.

vs. 31.8 μmol L^{-1}). Chl a was 2.4 μg L^{-1} in the shallow water and 2.9 μg L^{-1} in the deep water (Table 4), and PC:Chl a (μg C L^{-1}: μg Chl a L^{-1}) was 109 in the AASW and 91 in the mHSSW.

The fluorescence and freshness indices for DOM were 2% and 21% higher, respectively, in the mHSSW sample than the AASW sample while the humification index was 55% higher in the AASW sample (Table 4). The maximum excitation/emission of fluorescent DOM (Ex$_{max}$/Em$_{max}$) occurred in the range of tryptophan-like fluorescence (240/322-324 in the AASW and 240/334-352 in the mHSSW), and standardized maximum fluorescence revealed 1.7 times greater tryptophan-like fluorescence in the mHSSW sample compared with the AASW (Table 4).

The seafloor at the sample site was characterized by a rocky lag deposit, indicative of continuous or episodic strong bottom currents. Fine-grained sediment, including diatom frustules, was present interstitially between rocks and pebbles. The diatom assemblage recovered from near surficial sediments was characterized by Southern Ocean and Ross Sea pelagic species including *Eucampia antarctica*, *Thalassiosira oliverana*, *Thalassiosira tumida*, *Stelarima microtrias*, *Thalassiosira lentiginosa*, *Thlassiosira gracilis*, *Actinocyclus actinochilus*, and *Fragilariopsis obliquicostata*. Taxa characteristic of the northern polar frontal zone and lower latitudes, including *Thalassionema nitzschioides*, *Thalassiosira oestrupii* and *Actinocyclus octinarius*, were also represented. *Fragilariopsis curta* accounted for less than 1% of the diatom flora in the MIS sediment.

Bacterial and archaeal diversity and community structure

Microbial diversity, as indicated by the Shannon diversity index (H') and the inverse Simpsons diversity index ($1/\lambda$), was greatest in the >10 μm size fraction of the mHSSW sample (Table 5). Good's coverage, a non-parametric coverage estimator, indicated that the majority of the OTUs in the samples were identified through sequencing, (> 99%; Table 5) with projected 140 to 500 (calculated as 1/(1-Good's coverage)) more sequencing reads required to detect

Table 4. Fluorescence characteristics of dissolved organic matter (DOM) in the two water masses sampled. A higher fluorescence index indicates DOM of more microbial character, a higher humification index indicates a higher degree of humification, and a higher freshness index indicates a higher proportion of recently produced DOM. Standardized maximum fluorescence (Max Fluor) occurred in the region of tryptophan-like fluorescence for both samples (excitation 240 nm and emission 334–352 (30 m) and 322–334 (850 m)).

Sample	Fluorescence index	Humification index	Freshness index	Max fluor
AASW	1.65	0.31	1.35	0.56
mHSSW	1.70	0.14	1.72	0.97

an additional OTU from each sample (Fig. 4). The total numbers of OTUs observed in the SSU sequence libraries represented between 60% (mHSSW 0.2–3 μm size fraction) and 75% (mHSSW 3–10 μm size fraction) of the expected number of OTUs predicted by the Chao1 richness estimator (Table 5).

The three size fractions of mHSSW were dominated by phylotypes that classify within the Gammaproteobacteria and Bacteroidetes, with greater proportions of Bacteroidetes (predominantly Flavobacteria) occurring in the > 10 μm and 3–10 μm fractions relative to the 0.2–3 μm fraction (Fig. 4). Together, the Gammaproteobacteria and Bacteroidetes accounted for $\sim$ 53% of the OTUs in the mHSSW sample (size fractions pooled), with the Gammaproteobacteria alone accounting for nearly 75% of the OTUs observed at the sampling depth in the AASW. The most abundant operational taxonomic unit (OTU; 3.7% of sequence reads) in the mHSSW sample was most closely related (96% identity) to *Candidatus Vesicomyosocius okutanii*, a sulfide-oxidizing symbiont of a deep-sea clam. An OTU most closely related (98% sequence similarity) to the ammonia oxidizer *Nitrosopumilus maritimus*, was the third most common in the mHSSW sample, comprising 3.5% of

Table 5. Prokaryotic diversity estimates for the different water masses sampled. OTUs were calculated based on 97% similarity. H' = Shannon diversity index, $1/\lambda$ = inverse Simpsons diversity index. Good's coverage is a non-parametric coverage indicator. Chao1 gives the expected number of OTUs.

Sample	# of reads	# of OTUs	Good's coverage	Chao1	H'	$1/\lambda$
AASW	238448	1475	99.8%	2140	2.06	3.79
mHSSW 0.2–3 μm	193331	1805	99.6%	2995	4.26	23.37
mHSSW 3–10 μm	101768	2208	99.3%	2960	5.27	75.10
mHSSW > 10 μm	391658	3442	99.7%	4880	5.74	117.10
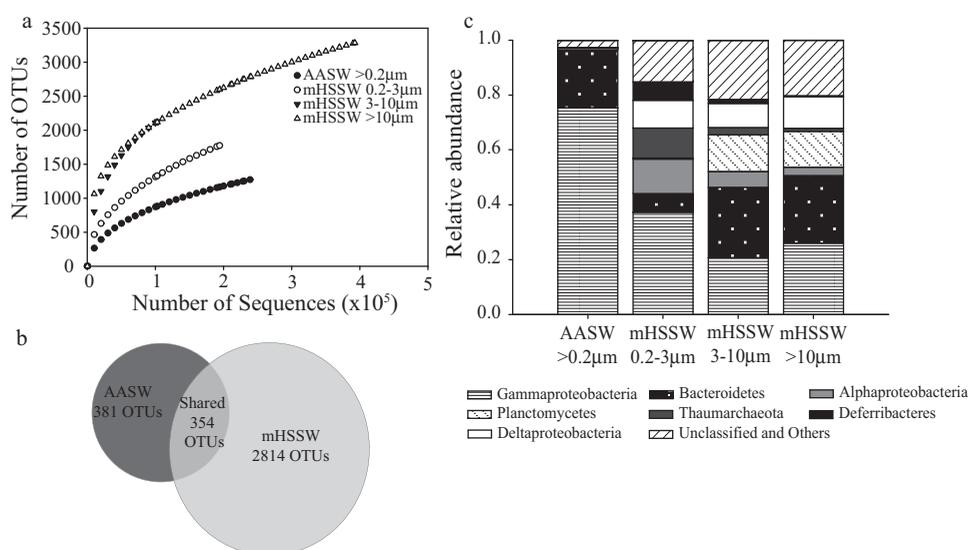
Fig. 4. (**a**) Rarefaction curves for OTU richness of samples from AASW (30 m) and mHSSW (850 m), (**b**) comparison of microbial communities from the AASW water mass and mHSSW water mass samples showing a 10% overlap in community composition at the OTU level (97% SSU sequence identity), (**c**) and relative abundance data for AASW and mHSSW.

total sequencing reads. Members of the Thuamarchaeota comprised a total of 4.1% of the mHSSW community (10.9%, 2.6%, and 1.3% of reads from the 0.2 μm to 3 μm, 3 μm to 10 μm and > 10 μm size fractions, respectively). The majority of sequences in the AASW were related to *Oceanospirillales* sp. (most abundant OTU, 42.4% of reads) and members of the SAR92 clade (second most abundant OTU, 28.9% of reads). OTUs most closely related to the SAR11 clade were rare, comprising 0.13% of the total library in the AASW and 1.2% in the mHSSW. A total of $\sim$ 9.0% of the sequence reads from the AASW were closely related to *Polaribacter* sp., a marine genus reported to possess gas vacuoles.

Approximately 10% of the OTUs identified in all samples were present in both the AASW and the mHSSW (Fig. 4). Eighteen of these OTUs were present at relative abundances > 0.1% in both water masses. In general, OTUs that were common in one water mass ($\geq$ 1%) were rare in the other water mass. Exceptions to this were in OTUs

related to the Oceanospirillaceae, which comprised 42.4% and 4.1% of the AASW and mHSSW populations, respectively, an OTU related to the SAR92 cluster (28.9% and 2.3% in the AASW and mHSSW, respectively), and Flavobacteriaceae (2.6% and 1.0% in the AASW and mHSSW, respectively).

Discussion

Sub-ice shelf habitats are among the least-studied ecosystems in the world's oceans. Our results show an active microbial ecosystem under the MIS, supported in part via chemoautotrophic activity and in part via advection of nutrients and biomass from eastern McMurdo Sound. Thick ice prevents the penetration of sunlight, leaving sub-ice shelf waters devoid of the primary production typical of open ocean photic zones, therefore horizontal advection from adjacent open waters should play a proportionally greater role in sub-ice shelf biogeochemistry. Sub-ice shelf habitats

can be oligotrophic, such as the J9 site beneath the RIS, (Lipps et al. 1979) where chemoautotrophically produced new carbon may be an important food source (Horrigan 1981). Conversely, the diverse assemblage that comprised the benthic community beneath the Amery Ice Shelf indicated a nutrient rich environment likely sustained by advection of phytoplankton produced organic matter (Riddle et al. 2007; Post et al. 2014). The J9 and Amery sites differ in their distance to open water ($\sim$ 400 km for J9 and $\sim$ 100 km for Amery). These results, along with those of our study, indicate that biogeochemical processes beneath an ice shelf are controlled by the proximity to open water, the trophic state of the source waters and new (chemoautotrophic) carbon production beneath the ice shelf.

Source of sub-MIS waters

The currents observed at our sampling site (Fig. 2b) are in agreement with previous observations of a strong southward flow component from the Ross Sea to the MIS via the eastern side of McMurdo Sound (Robinson et al. 2010). Our biological and physicochemical measurements support an eastern McMurdo Sound source for the sub-MIS waters at our sample site. Bacterioplankton abundances in eastern McMurdo Sound were similar to those at our site (Table 2; $\sim 10^8$ cells L^{-1}, Hodson et al. 1981; Rivkin 1991). In contrast, the oligotrophic western side, which is a mixture of sub-MIS outflow and water circulating from the Ross Sea, contained an order of magnitude fewer cells (Hodson et al. 1981). Nutrient concentrations (SRP and DIN; Table 1) were within a few μmol L^{-1} of those measured during December in eastern McMurdo Sound (Rivkin 1991). These data imply that the transport time from the open waters of McMurdo Sound to our sample site ($\sim$ 2 d; Robinson 2004) did not result in major changes to the concentrations of inorganic nutrients or microbial cells. Given the similarity between the biological and physicochemical character of our samples and eastern McMurdo Sound waters and the prevailing current direction we conclude that nutrient and biomass-rich water advected from eastern McMurdo Sound likely plays an important role in sub-MIS biogeochemical processes.

Sedimentary diatoms can also provide tracers of water column advection, however, strong bottom currents (Fig. 2b) at our sample site suggest that little deposition occurs there at present. The most common diatoms we observed (multiple species of Thalassiosira, A. actinochilus, and F. obliquicostata) are also found in sediments from the eastern side of McMurdo Sound (Leventer and Dunbar 1988), however the near absence of F. curta, which is commonly observed in McMurdo Sound, is striking. No viable diatoms were recovered in our surface sediment samples, suggesting that the diatoms we observed may represent earlier deposition, or that they are the result of advection from pelagic sources. Together, these data indicate that diatom deposition may

not be an accurate tracer of modern water sources at this site.

Organic carbon sources

Sub-ice shelf systems are unique from open ocean environments in their dependence on horizontal advection of food sources or in situ chemoautotrophic production, rather than on vertical fluxes of phytoplankton-derived food sources (Gutt et al. 2011). To determine whether intact phytoplankton cells are advected beneath the MIS, and consider their potential importance as a food source, we examined Chl a concentrations and phytoplankton abundances in the AASW and mHSSW. Chl a concentrations in both samples were similar to values measured in McMurdo Sound during mid-December (Rivkin 1991), suggesting that phytoplankton loss rates (i.e., due to sedimentation, cell lysis, grazing) were low by the time water from McMurdo Sound reached our sampling site. Our CTD data revealed the presence of three distinct water masses beneath the MIS, rather than a well-mixed water column that would result in even distribution of Chl a, so the simplest explanation for the similar concentrations of Chl a we measured in the AASW and mHSSW (2.4 μg L^{-1} and 2.9 μg L^{-1}, respectively) is settling of Chl a containing cells into the aphotic mHSSW during the $\sim$ 2 d transport time to our sample site.

Indeed, our flow cytometry and microscopy data showed that Chl a containing phytoplankton cells were present in both water masses. Phytoplankton cells were larger in the mHSSW than in the AASW and had higher Chl a emission per cell, suggesting that intact cells or colonies were transported to depth, a phenomenon that has been previously reported for P. antarctica (DiTullio et al. 2000). The PC:Chl a (μg L^{-1}: μg L^{-1}) measured in our samples (109 in the AASW and 91 in the mHSSW) was similar to that measured in active populations from the Ross Sea (92; Ditullio and Smith 1996), supporting our contention that cells transported to depth were intact. Intact phytoplankton cells can be advected great distances under ice from open water (Holm-Hansen et al. 1978), where they may later be decomposed as a source of nutrition for heterotrophic growth of sub-ice shelf microorganisms.

To our knowledge, no measurements of P. antarctica decomposition rates have been made for the MIS/RIS cavity, although DiTullio et al. (2000) tracked P. antarctica export in the Ross Sea and showed that intact cells are rapidly exported to depth. Based on a phytoplankton decomposition rate of 0.032% d^{-1} for a cold saline Antarctic lake near McMurdo Sound (Priscu 1992), 100% of the phytoplankton particulate carbon we observed would be decomposed after 10 yr. This potential decadal scale decomposition suggests that sinking and advected phytoplankton are important sources of organic matter beneath the ice shelf, and may continue to be as they are advected farther from the ice shelf front.

Bulk DOC concentrations in our samples were relatively low, similar to Ross Sea wintertime background concentrations (e.g., Ducklow 2003). Based on our determinations of bacterial growth efficiency and bacterial carbon production, the heterotrophic bacterial carbon demand (bacterial carbon production + bacterial carbon respiration) in our samples was $\sim$ 50–90 nmol C L^{-1} d^{-1}. Assuming that the entire DOC pool is bioavailable and the system in steady-state, these rates would be expected to deplete the standing stock of DOC within 1–2 yr. The total DOC pool is likely an overestimate of the bioavailable fraction, as the labile pool is consumed quickly, concurrent with the phytoplankton bloom (Ducklow 2003). Residence times in the MIS/RIS cavity may vary between water masses and are not well constrained, but estimates range from $\sim$ 2 yr to 8 yr (Smethie and Jacobs 2005; Reddy et al. 2010). Based on this, our data imply that another organic carbon source would be required to maintain heterotrophic potential beneath the ice shelf during the water residence time.

The production of organic matter via fixation of CO_2 into biomass (chemoautotrophy) may also be important under the ice. Our microbial diversity, in concert with results from other studies (e.g., Gryzmski et al. 2012; Williams et al. 2012; Christner et al. 2014) show that aerobic ammonia-oxidizing microorganisms are widespread in Antarctic aquatic environments, and may be key sources of new organic carbon to ecosystems shielded from sunlight. Isolated representatives of the proposed phylum Thaumarchaeota, a major group identified in our mHSSW sample, are aerobic ammonia oxidizers that fix CO_2 (Könneke et al. 2014). We measured dark CO_2 fixation of $\sim$ 3 nmol C L^{-1} d^{-1} in the 0.2–3 μm size fraction in both the shallow AASW and deep mHSSW samples. We attribute this CO_2 fixation to bacteria and/or archaea, rather than phytoplankton-mediated anapleurotic reactions because our flow cytometry data showed that the 0.2–3 μm size fraction was chiefly comprised of bacterioplankton. Still, dark CO_2 fixation was an order of magnitude less than heterotrophic bacterial carbon production at our study site, implying that heterotrophic demand in this region of the MIS must also rely on some combination of the previously discussed carbon sources (advected organic matter and biomass or the DOC pool).

Dissolved organic matter quality and microbial growth

Dissolved organic carbon concentrations, while higher in the surface waters (42.1 μmol L^{-1}) than at depth (31.8 μM) were similar to Ross Sea wintertime background values (40–42 μmol L^{-1}; Ducklow 2003). With terrestrial sources limited by a paucity of land plants, autochthonous production dominates the DOM pool in Antarctic waters (e.g., McKnight et al. 2001). Fluorescence indices derived from our EEMS datasets were consistent with those of microbially produced organic matter, where a high index ($\sim$ 1.8) corresponds to DOM of microbial origin, and a low index ($\sim$ 1.2) corre-

sponds to DOM of terrestrial origin (McKnight et al. 2001; Cory and McKnight 2005). Humification indices increase with the presence of more humified and/or older DOM (up to > 10 for fulvic acids; Zsolnay et al. 1999), while a Freshness index > 1 corresponds to recently produced microbial DOM (Huguet et al. 2009). Both the humification and freshness indices calculated for our samples are consistent with DOM of recent microbial origin. The 55% higher humification and 22% lower freshness indices in the AASW water mass relative to the deeper mHSSW water mass reveal that the near-surface DOM was more degraded, perhaps due to high rates of heterotrophic activity associated with phytoplankton production in the photic zone of McMurdo Sound before being advected into the sub-ice cavity.

Ducklow (2003) showed that labile DOC produced during the summer Ross Sea phytoplankton bloom is quickly consumed, leaving a mainly recalcitrant pool available for consumption during the winter. This is consistent with our findings of more degraded near-surface DOM. All three indices of biological activity (^{3}H-TdR, ^{3}H-Leu, and ^{14}C-bicarbonate uptake) revealed increased metabolic rates in the deeper mHSSW water mass. Increased biological activity may explain the stronger signal for freshly produced DOM, including the elevated maximum tryptophan-like fluorescence in the mHSSW relative to the AASW.

Although the ability to take up leucine and thymidine can differ among bacterial groups (Pérez et al. 2010), the ratio of Leu (protein production or biomass maintenance) to TdR (DNA synthesis or cell division) incorporation rates can be used as a metric for understanding changes in rates of biomass maintenance relative to reproduction (Chin-Leo and Kirchman 1988; Shiah and Ducklow 1997; Vick and Priscu 2012). The lower Leu: TdR we detected in the mHSSW sample may indicate faster heterotrophic bacterioplankton growth rates at depth relative to the surface, possibly a product of the availability of higher quality DOM.

Conclusions

The sub-McMurdo Ice Shelf cavity provides an important conduit for organisms and nutrients between the Ross Sea and the sub-Ross Ice Shelf cavity. Our results show that the decomposition of phytoplankton coupled with chemoautotrophic production of new carbon may be important in supporting ecosystems beneath the MIS. While inputs from phytoplankton blooms are available only during the austral summer, chemoautotrophic production is available year-round. Our sequence-based community analysis corroborates our contention and those of previous reports suggesting that new carbon produced by chemoautotrophic ammonia-oxidizing organisms can supply organic carbon to partially sustain ecosystem processes beneath Antarctic ice shelves such as the MIS and RIS. Other abundant phylotypes in our deep-water sample are related to a chemoautotrophic sulfide

oxidizer, suggesting that reduced sulfur compounds may also be an important energy source to fuel chemoautotrophic production beneath the MIS.

Given that many of the ice shelves surrounding Antarctica's coastline are thinning at increasing rates (Paolo et al. 2015) and are susceptible to collapse (Joughin et al. 2014), their losses should lead to significant changes in the biogeochemistry of Antarctic coastal systems supported by sub-ice shelf processes. Changes in Southern Ocean ice cover can impact carbon biogeochemistry at local as well as global (see review by Sigman et al. 2010) scales. In the case of the RIS/ MIS, the relative biogeochemical importance of chemoautotrophic production and material advected beneath the ice from the Ross Sea would decrease if photosynthetic primary production began to occur in newly open water. Assuming that the rates we measured are relatively constant over the year, the sum of heterotrophic and autotrophic C production under the MIS is currently $< 1\%$ of the photosynthetic C production in the open water of the Ross Sea (per km^2 per year in the top 100 m of water column; Ross Sea estimates in Arrigo et al. 2008). Considering such disparity in productivity between ice shelf covered and open water, the loss of ice shelves can be expected to have cascading effects on elemental cycling in the region via shifts in dominant biological processes. In a less dramatic scenario than massive ice-shelf loss, climate change induced changes to winds and temperatures that modulate incursions of Circumpolar Deep Water onto the continental shelf could severely disrupt the Ross Sea food web (Smith et al. 2014), leading to major effects on sub-MIS biogeochemistry. Baseline data from existing sub ice shelf environments, such as the MIS, inform the prediction of the biogeochemical impacts of ice shelf collapse and climate change in the Southern Ocean.

References

Apprill, A., S. McNally, R. Parsons, and L. Weber. 2015. Minor revision to V4 region SSU rRNA 806R gene primer greatly increases detection of SAR11 bacterioplankton. Aquat. Microb. Ecol. **75**: 129–137. doi:10.3354/ame01753

Arrigo, K. R. 1999. Phytoplankton community structure and the drawdown of nutrients and CO_2 in the Southern Ocean. Science **283**: 365–367. doi:10.1126/science.283.5400.365

Arrigo, K. R., and C. R. McClain. 1994. Spring phytoplankton production in the Western Ross Sea. Science **266**: 261–263. doi:10.1126/science.266.5183.261

Arrigo, K. R., and G. L. van Dijken. 2004. Annual changes in sea-ice, chlorophyll a, and primary production in the Ross Sea, Antarctica. Deep-Sea Res. Part II Top. Stud. Oceanogr. **51**: 117–138. doi:10.1016/j.dsr2.2003.04.003

Arrigo, K. R., G. L. van Dijken, and S. Bushinsky. 2008. Primary production in the Southern Ocean, 1997–2006. J. Geophys. Res. **113**: C08004. doi:10.1029/2007JC004551

Azam, F., J. R. Beers, L. Campbell, A. F. Carlucci, O. Holm-Hansen, F. M. Reid, and D. M. Karl. 1979. Occurrence and

metabolic activity of organisms under the Ross Ice Shelf, Antarctica, at Station J9. Science **203**: 451–453. doi:10.1126/science.203.4379.451

Barry, J. P. 1988. Hydrographic patterns in McMurdo Sound, Antarctica and their relationship to local benthic communities. Polar Biol. **8**: 377–391. doi:10.1007/BF00442029

Bell, R. T. 1993. Estimating production of heterotrophic bacterioplankton via incorporation of tritiated thymidine. *In* P. F. Kemp, B. F. Sherr, E. B. Sherr and J. J. Cole [eds.], Handbook of methods in aquatic microbial ecology. Lewis Publishers.

Bertolin, M., and I. Schloss. 2009. Phytoplankton production after the collapse of the Larsen A Ice Shelf, Antarctica. Polar Biol. **32**: 1435–1446. doi:10.1007/s00300-009-0638-x

Blythe, D., D. V. Duling, and D. E. Gibson. 2014. Developing a hot-water drill system for the WISSARD project: 2. In situ water production. Ann. Glaciol. **55**: 298–302. doi:10.3189/2014AoG68A037

Bouvier, T., P. A. Del Giorgio, and J. M. Gasol. 2007. A comparative study of the cytometric characteristics of high and low nucleic-acid bacterioplankton cells from different aquatic ecosystems. Environ. Microbiol. **9**: 2050–2066. doi:10.1111/j.1462-2920.2007.01321.x

Budillon, G., P. Castagno, S. Aliani, G. Spezie, and L. Padman. 2011. Thermohaline variability and Antarctic bottom water formation at the Ross Sea shelf break. Deep-Sea Res. Part I Oceanogr. Res. Pap. **58**: 1002–1018. doi:10.1016/j.dsr.2011.07.002

Burnett, J., and others. 2014. Developing a hot-water drill system for the WISSARD project: 3. Instrumentation and control systems. Ann. Glaciol. **55**: 303–310. doi:10.3189/2014AoG68A039

Caporaso, J. G., and others. 2012. Ultra-high-throughput microbial community analysis on the Illumina HiSeq and MiSeq platforms. ISME J. **6**: 1621–1624. doi:10.1038/ismej.2012.8

Carr, S. A., and others. 2013. Bacterial abundance and composition in marine sediments beneath the Ross Ice Shelf, Antarctica. Geobiology **11**: 377–395. doi:10.1111/gbi.12042

Celussi, M., A. Bergamasco, B. Cataletto, S. F. Umani, and P. Del Negro. 2010. Water masses' bacterial community structure and microbial activities in the Ross Sea, Antarctica. Antarct. Sci. **22**: 361–370. doi:10.1017/S0954102010000192

Chao, A. 1984. Non-parametric estimation of the number of classes in a population. Scand. J. Stat. **11**: 265–270. http://www.jstor.org/stable/4615964

Chin-Leo, G., and D. Kirchman. 1988. Estimating bacterial production in marine waters from the simultaneous incorporation of thymidine and leucine. Appl. Environ. Microbiol. **8**: 1934–1939.

Christner, B. C., and others. 2006. Limnological conditions in Subglacial Lake Vostok, Antarctica. Limnol. Oceanogr. **6**: 2485–2501. doi:10.4319/lo.2006.51.6.2485

Christner, B. C., and others. 2014. A microbial ecosystem beneath the West Antarctic ice sheet. Nature **512**: 310–313. doi:10.1038/nature13667

Clough, J. W., and B. L. Hansen. 1979. The Ross Ice Shelf Project. Science **203**: 433–434. doi:10.1126/science.203.4379.433

Cory, R. M., and D. M. McKnight. 2005. Fluorescence spectroscopy reveals ubiquitous presence of oxidized and reduced quinones in dissolved organic matter. Environ. Sci. Technol. **39**: 8142–8149. doi:10.1021/es0506962

Daly, M., F. Rack, and R. Zook. 2013. *Edwardsiella andrillae*, a new species of sea anemone from Antarctic Ice. PLoS One **8**: e83476. doi:10.1371/journal.pone.0083476

del Giorgio, P. A., R. Condon, T. Bouvier, K. Longnecker, C. Bouvier, E. Sherr, and J. M. Gasol. 2011. Coherent patterns in bacterial growth, growth efficiency, and leucine metabolism along a northeastern Pacific inshore-offshore transect. Limnol. Oceanogr. **1**: 1–16. doi:10.4319/lo.2011.56.1.0001

Depoorter, M. A., J. L. Bamber, J. A. Griggs, J. T. M. Lenaerts, S. R. M. Ligtenberg, M. R. van den Broeke, and G. Moholdt. 2013. Calving fluxes and basal melt rates of Antarctic ice shelves. Nature **502**: 89–92. doi:10.1038/nature12567

DiTullio, G. R., and W. O. Smith. 1996. Spatial patterns in phytoplankton biomass and pigment distributions in the Ross Sea. J. Geophys. Res. **101**: 18467. doi:10.1029/96JC00034

DiTullio, G. R., and others. 2000. Rapid and early export of *Phaeocystis antarctica* blooms in the Ross Sea, Antarctica. Nature **404**: 595–598. doi:10.1038/35007061

Domack, E., A. Leventer, S. Sylva, V. Wilmott, and B. Huber. 2005. A chemotrophic ecosystem found beneath Antarctic ice shelf. Trans. Am. Geophys. Union **86**: 269–276. doi:10.1029/2005EO290001

Ducklow, H. W. 2003. Seasonal production and bacterial utilization of DOC in the Ross Sea, Antarctica. *In* G. R. Ditullio and R. B. Dunbar [eds.], Biogeochemistry of the Ross Sea. American Geophysical Union.

Ducklow, H., C. Carlson, M. Church, D. Kirchman, D. Smith, and G. Steward. 2001. The seasonal development of the bacterioplankton bloom in the Ross Sea, Antarctica, 1994–1997. Deep-Sea Res. II **48**: 4199–4221. doi:10.1016/S0967-0645(01)00086-8

Fillinger, D., D. Janussen, T. Lundälv, and C. Richter. 2013. Rapid glass sponge expansion after climate-induced Antarctic ice shelf collapse. Curr. Biol. **23**: 1330–1334. doi:10.1016/j.cub.2013.05.051

Fox, A. J., and A. P. R. Cooper. 1994. Measured properties of the Antarctic ice sheet derived from the SCAR Antarctic digital database. Polar Record **30**: 201–206. doi:10.1017/S0032247400024268

Fuhrman, J., and F. Azam. 1982. Thymidine incorporation as a measure of heterotrophic bacterioplankton production in marine surface waters: Evaluation and field results. Mar. Biol. **66**: 109–120. doi:10.1007/BF00397184

Gasol, J. M., and P. A. del Giorgio. 2000. Using flow cytometry for counting natural planktonic bacteria and understanding the structure of planktonic bacterial communities. Sci. Mar. **64**: 197–224.

Gilmour, A. 1979. Ross ice shelf sea temperatures. Science **203**: 438–439. doi:10.1126/science.203.4379.438

Good, I. J. 1953. The population frequencies of species and the estimation of population parameters. Biometrika **40**: 237–264. doi:10.1093/biomet/40.3-4.237

Greischar, L. L., and C. R. Bently. 1980. Isostatic equilibrium grounding line between the West Antarctic inland ice sheet and the Ross Ice Shelf. Nature **283**: 651–654. doi:10.1038/283651a0

Griggs, J., and J. Bamber. 2011. Antarctic ice-shelf thickness from satellite radar altimetry. J. Glaciol. **57**: 485–498. doi:10.3189/002214311796905659

Gryzmski, J. J., and others. 2012. A metagenomic assessment of winter and summer bacterioplankton from Antarctica Peninsula coastal surface waters. ISME J. **2**: 1–15. doi:10.1038/ismej.2012.28

Gutt, J., and others. 2011. Biodiversity change after climate-induced ice-shelf collapse in the Antarctic. Deep-Sea Res. Part II **58**: 74–83. doi:10.1016/j.dsr2.2010.05.024

Hillebrand, H., C. D. Dürselen, D. Kirschtel, U. Pollingher, and T. Zohary. 1999. Biovolume calculation for pelagic and benthic microalgae. J. Phycol. 424: 403–424. doi:10.1046/j.1529-8817.1999.3520403.x

Hodson, R., F. Azam, A. F. Carlucci, J. A. Fuhrman, D. M. Karl, and O. Holm-Hansen. 1981. Microbial uptake of dissolved organic matter in McMurdo Sound, Antarctica. Mar. Biol. **61**: 89–94. doi:10.1007/BF00386648

Holm-Hansen, O., F. Azam, L. Campbell, A. F. Carlucci, and D. M. Karl. 1978. Microbial life beneath the Ross Ice Shelf. Antarct. J. U.S. **4**: 129–130.

Horgan, H. J., and others. 2013. Estuaries beneath ice sheets. Geology **11**: 1159–1162. doi:10.1130/G34654.1

Horrigan, S. G. 1981. Primary production under the Ross Ice Shelf, Antarctica. Limnol. Oceanogr. **26**: 378–382. doi:10.4319/lo.1981.26.2.0378

Huguet, A., L. Vacher, S. Relexans, S. Saubusse, J. M. Froidefond, and E. Parlanti. 2009. Properties of fluorescent dissolved organic matter in the Gironde Estuary. Org. Geochem. **40**: 706–719. doi:10.1016/j.orggeochem.2009.03.002

IOC, SCOR, and IAPSO. 2010. The international thermodynamic equation of seawater—2010: Calculation and use of thermodynamic properties. Intergovernmental Oceanographic Commission, Manuals and Guides. UNESCO.

Jacobs, S. S., A. F. Amos, and P. M. Bruchhausen. 1970. Ross Sea oceanography and Antarctic bottom water formation. Deep-Sea Res. Oceanogr. Abstr. **17**: 935–962. doi:10.1016/0011-7471(70)90046-X

Jacobs, S. S., A. L. Gordon, and J. L. Ardai, Jr. 1979. Circulation and melting beneath the Ross ice shelf. Science **203**: 439–443. doi:10.1126/science.203.4379.439

Jacobs, S. S., and R. G. Fairbanks. 1985. Origin and evolution of water masses near the Antarctic continental margin: Evidence from $H_2{}^{18}O/H_2{}^{16}O$ ratios in seawater. Antarct. Res. Ser. **43**: 59–85. doi:10.1029/AR043p0059

Joughin, I., B. Smith, and B. Medley. 2014. Marine ice sheet collapse potentially underway for the Thwaites Glacier Basin, West Antarctica. Science **344**: 735–738. doi: 10.1126/science.1249055

Kepner, R., R. Wharton, and C. Suttle. 1988. Viruses in Antarctic Lakes. Limnol. Oceanogr. **7**: 1754–1761. http://www.jstor.org/stable/2839057

Kirchman, D., E. K'nees, and R. Hodson. 1985. Leucine incorporation and its potential as a measure of protein synthesis by bacteria in natural aquatic systems. Appl. Environ. Microbiol. **49**: 599–607.

Lebaron, P., P. Servais, H. Agogué, F. Joux, H. Agogue, and C. Courties. 2001. Does the high nucleic acid content of individual bacterial cells allow us to discriminate between active cells and inactive cells in aquatic systems? Appl. Environ. Microbiol. **67**: 1775–1782. doi:10.1128/AEM.67.4.1775-1782.2001

Leventer, A., and R. Dunbar. 1988. Recent diatom record of McMurdo Sound, Antarctica: Implications for history of sea ice extent. Paleoceanography **3**: 259–274. doi:10.1029/PA003i003p00259

Lipps, J. H. H., T. E. Ronan, T. E. E. Delaca, and T. E. Ronan, Jr. 1979. Life below the Ross ice shelf, Antarctica. Science **203**: 447–449. doi:10.1126/science.203.4379.447

Lisle, J. T., and J. C. Priscu. 2004. The occurrence of lysogenic bacteria and microbial aggregates in the lakes of the McMurdo Dry Valleys, Antarctica. Microb. Ecol. **47**: 427–439. doi:10.1007/s00248-003-1007-x

Magurran, A. 1988. Ecological diversity and its measurement. Princeton Univ. Press.

Marie, D., F. Partensky, D. Vaulot, and C. Brussaard. 2001. Enumeration of phytoplankton, bacteria, and viruses in marine samples. Curr. Protoc. Cytom. **10**: 11.11:11.11.1–11.11.15. doi:10.1002/0471142956.cy1111s10

Mcknight, D. M., and others. 2001. Spectrofluorometric characterization of dissolved organic matter for indication of precursor organic material and aromaticity. Limnol. Oceanogr. **46**: 38–48. doi:10.4319/lo.2001.46.1.0038

Montagnes, D. J. S., J. A. Berges, P. J. Harrison, and F. J. R Taylor. 1994. Estimating carbon, nitrogen, protein, and chlorophyll a from volume in marine phytoplankton. Limnol. Oceanogr. **39**: 1044–60. doi:10.4319/lo.1994.39.5.1044

Paolo, F. S., H. A. Fricker, and L. Padman. 2015. Volume loss from Antarctic ice shelves is accelerating. Science **348**: 327–331. doi:10.1126/science.aaa0940

Pérez, M., P. Hörtnagl, and R. Sommaruga. 2010. Contrasting ability to take up leucine and thymidine among freshwater bacterial groups: Implications for bacterial production measurements. Environ. Microbiol. **12**: 74–82. doi:10.1111/j.1462-2920.2009.02043.x

Post, A. L., and others. 2014. Modern sedimentation, circulation and life beneath the Amery Ice Shelf, East Antarctica. Cont. Shelf Res. **74**: 77–87. doi:10.1016/j.csr.2013.10.010

Priscu, J. C. 1992. Particulate organic matter decomposition in the water column of Lake Bonney, Taylor Valley. Antarct. J. U.S. **27**: 260.

Rack, F. R., and others. 2014. Developing a hot-water drill system for the WISSARD project: 1. Basic drill system components and design. Ann. Glaciol. **55**: 285–297. doi:10.3189/2014AoG68A031

Reddy, T. E., D. M. Holland, and K. R. Arrigo. 2010. Ross ice shelf cavity, circulation, residence time, and melting: Results from a model of oceanic chlorofluorocarbons. Cont. Shelf Res. **7**: 733–742. doi:10.1016/j.csr.2010.01.007

Riddle, M. J., M. Craven, P. M. Goldsworthy, and F. Carsey. 2007 A diverse benthic assemblage 100 km from open water under the Amery Ice Shelf, Antarctica. Paleoceanography **22**: PA1204. doi:10.1029/2006PA001327

Rignot, E., S. Jacobs, J. Mouginot, and B. Scheuchl. 2013. Ice-shelf melting around Antarctica. Science **341**: 266–269. doi:10.1126/science.1235798

Rivkin, R. B. 1991. Seasonal patterns of planktonic production in McMurdo Sound, Antarctica. Am. Zool. **16**: 5–16. doi:10.1093/icb/31.1.5

Robinson, N. J. 2004. An oceanographic study of the cavity beneath the McMurdo Ice Shelf, Antarctica. M.S. thesis. Victoria Univ. of Wellington, New Zealand.

Robinson, N. J., M. J. M. Williams, P. J. Barrett, and A. R. Pyne. 2010. Observations of flow and ice-ocean interaction beneath the McMurdo Ice Shelf, Antarctica. J. Geophys. Res. **115**: C03025. doi:10.1029/2008JC005255

Scherer, R. P. 1991. Quaternary and tertiary microfossils from beneath Ice Stream B: Evidence for a dynamic West Antarctic Ice Sheet history. Palaeogeogr. Palaeocl. **90**: 395–412. doi:10.1016/S0031-0182(12)80038-1

Schlitzer, R. 2013. Ocean Data View. Available from http://odv.awi.de

Schloss, P. D., and others. 2009. Introducing mothur: Open-source, platform-independent, community-supported software for describing and comparing microbial communities. Appl. Environ. Microbiol. **75**: 7537–7541. doi:10.1128/AEM.01541-09

Schneider, C. A., W. S. Rasband, and K. W. Eliceiri. 2012. NIH Image to ImageJ: 25 years of image analysis. Nature Methods 7: 671–675. doi:10.1038/nmeth.2089

Shiah, F. K., and H. W. Ducklow. 1997. Bacterioplankton growth responses to temperature and chlorophyll variations in estuaries measured by thymidine:leucine incorporation ratio. Aquat. Microb. Ecol. **13**: 151–159. doi:10.3354/ame013151

Sigman, D., M. Hain, and G. Haug. 2010. The polar ocean and glacial cycles in atmospheric CO2 concentration. Nature **466**: 47–55. doi:10.1038/nature09149

Smethie, W., Jr., and S. Jacobs. 2005. Circulation and melting under the Ross ice shelf: Estimates from evolving CFC, salinity and temperature fields in the Ross Sea. Deep-Sea Res. Part I. **6**: 959–978. doi:10.1016/j.dsr.2004.11.016

Smith, W. O., Jr., and L. I. Gordon. 1997. Hyperproductivity of the Ross Sea (Antarctica) polynya during austral spring. Geophys. Res. Lett. **24**: 233–236. doi:10.1029/96GL03926

Smith, W., and J. Comiso. 2008. Influence of sea ice on primary production in the Southern Ocean: A satellite perspective. J. Geophys. Res. Oceans **C5**: C05S93. doi:10.1029/2007JC004251

Smith, W. O., Jr., P. N. Sedwick, K. R. Arrigo, D. G. Ainley, and A. H. Orsi. 2012. The Ross Sea in a sea of change. Oceanography **25**: 90–103. doi:10.5670/oceanog.2012.80

Smith, W. O., Jr., M. S. Dinniman, E. E. Hofmann, and J. M. Klinck. 2014. The effects of changing winds and temperatures on the oceanography of the Ross Sea into the 21st century. Geophys. Res. Lett. **41**: 1624–1631. doi:10.1002/2014GL059311

Solórzano, L. 1969. Determination of ammonia in natural waters by the phenolhypochlorite method. Limnol. Oceanogr. **5**: 799–801. doi:10.4319/lo.1969.14.5.0799

Stover, C. 2006. A new account of Ross Sea water: Characteristics, volumetrics, and variability. Thesis. Texas A&M University.

Strickland, J., and T. Parsons. 1968. A practical handbook of seawater analysis. Fisheries Research Board of Canada. Ottowa.

Takacs, C., and J. Priscu. 1998. Bacterioplankton dynamics in the McMurdo Dry Valley lakes, Antarctica: Production and biomass loss over four seasons. Microb. Ecol. **3**: 239–250. doi:10.1007/s002489900111

Vick, T. J., and J. C. Priscu. 2012. Bacterioplankton productivity in lakes of the Taylor Valley, Antarctica, during the polar night transition. Aquat. Microb. Ecol. **68**: 77–90. doi:10.3354/ame01604

Welschmeyer, N. 1994. Fluorometric analysis of chlorophyll a in the presence of chlorophyll b and pheopigments. Limnol. Oceanogr. **8**: 1985–1992. doi:10.4319/lo.1994.39.8.1985

Williams, R., and E. Robinson. 1979. Ocean tide and waves beneath the Ross ice shelf, Antarctica. Science **203**: 443–445. doi:10.1126/science.203.4379.443

Williams, T. J., and others. 2012. A metaproteomic assessment of winter and summer bacterioplankton from Antarctic Peninsula coastal surface waters. ISME J. **6**: 1883–1900. doi:10.1038/ismej.2012.28

Wouters, B., and others. 2015. Dynamic thinning of glaciers on the Southern Antarctic Peninsula. Science **348**: 899–903. doi:10.1126/science.aaa5727

Yakimov, M. M., and others. 2011. Contribution of crenarchaeal autotrophic ammonia oxidizers to the dark primary production in Tyrrhenian deep waters (Central Mediterranean Sea). ISME J. **5**: 945–961. doi:10.1038/ismej.2010.197

Zsolnay, A., E. Baigar, M. Jimenez, B. Steinwg, and F. Saccomandi. 1999. Differentiating with fluorescence spectroscopy the sources of dissolved organic matter in soils subjected to drying. Chemosphere **38**: 45–50. doi:10.1016/S0045-6535(98)00166-0